Supplementary Information (SI) for ChemComm.

Ultra-high Li+ transfer efficiency of in-situ grown membrane for high-performance batteries

Jian Wang,[a] Kang Ma,[b] Yanbo Zhang,[a] Jiawei Chen,[a] Xin Song,[a*] Jianmin Zhang [a*]

a.College of Mechanical and Electrical Engineering, Power & Energy Storage System Research Center, Qingdao University, Qingdao, 266071, China

b.School of Materials Science and Engineering, Qingdao University, Qingdao, 266071, China

Materials

MgO nanoparticles were purchased from Jiangsu Xianfeng Nanomaterials Technology Co., Ltd. Cellulose acetate (CA) and $LiFePO_4$ (battery grade) were purchased from Shanghai Aladdin Biochemical Technology Co., Ltd. PVDF (Solef 6010) was purchased from Solvay Co., Ltd. (Tavaux, France). N, N-dimethylformamide (DMF, analytical grade), and aluminum nitrate nonahydrate ($Al(NO_3)_3 \cdot 9H_2O$) were bought from Sinopharm Chemical Reagent Co., Ltd. (Shanghai, China). N-methyl-2-pyrrolidone (NMP, analytical grade) and 1 mol/L $LiPF_6$ (in EC: DEC = 1:1 v/v) were bought from Suzhou Duoduo Chemical Technology (Suzhou, China) Co., Ltd. Super P (battery grade) and PVDF (HSV 900) were purchased from Shenzhen Tianchenghe Technology Co., Ltd. The samples used for comparison were commercial PP (Celgard 2500, Charlotte, NC, USA). All materials were used as received without any further modification.

Preparation of PVDF-CA/Mg-Al_2O_3 composite membrane

First, 0.11 g of MgO was dissolved in 7 mL of N, N-dimethylformamide (DMF) and ultrasonicated under room-temperature. The aim is to achieve uniform dispersion of MgO nanoparticles within the DMF. Next, 1.00 g of PVDF and 0.20 g of CA were added to the well-dispersed suspension. Finally, the suspension of the mixtures was stirred at 50 °C for 3 h to make a blended slurry.

After degassing at 30 °C for 2 h, the slurry was cast onto a glass plate using a doctor blade. Then, the plate was immersed in $Al(NO_3)_3$ salt solution to start a non-solvent phase separation process, the PVDF-CA/Mg-Al_2O_3 composite membrane was finally obtained after drying in a vacuum oven at 60 °C for 12 h.

During the phase separation process, MgO reacts with $Al(NO_3)_3$ salt solution, producing $Al(OH)_3$ and $Mg(OH)_2$. The reaction is mainly determined by the solubility product constant (Ksp)[1]. Since the formation of $Al(OH)_3$ ($Ksp=1.9*10^{-33}$) is more preferred than $Mg(OH)_2$ ($Ksp=1.5*10^{-11}$), the chemical formula is shown in **CR (1)**. The theoretical evidence for this reaction is deduced from a previous study[1].

$$MgO_{(S)}+Al^{3+}_{(aq)}+H_2O \rightarrow Mg^{2+}_{(aq)}+Al(OH)_{3\,(S)} \qquad (CR1)$$

The PVDF membranes with mixed CA only, mixed CA with MgO, and directly doped Al_2O_3, which were all immersed in water for phase separation, are named as PVDF-CA, PVDF-CA/MgO, and PVDF-CA/Al_2O_3, respectively. The composite membranes produced by different Mg: Al molar ratios (phase separation in $Al(NO_3)_3$ salt solution) are named as PVDF-CA/Mg-Al(31), PVDF-CA/Mg-Al(21), and PVDF-CA/Mg-Al_2O_3, respectively.

Physical characterizations

1. The morphologies and microstructures of the composite membranes were analyzed using a scanning electron microscope (SEM, JSM-6390LV, Tokyo, Japan) at an accelerating voltage of 15 kV, coupled with energy-dispersive spectroscopy (EDS). X-ray diffraction (XRD, Ultima IV, Tokyo, Japan) was carried out to analyze the crystalline structure of substances at diffraction angles ranging from 10−80°. Fourier transform infrared spectroscopy (FTIR) was conducted using an infrared spectrometer (Nicolet iS50, USA) in the range of 400−4000 cm^{-1}. Inductively coupled plasma mass (ICP) was conducted using an ICP-OES/MS (5110 OES, USA) to

analyze elements both qualitatively and quantitatively. The mechanical properties of the samples were examined by a universal testing machine (UTM4104X, SUNS, China) with a gauge length of 2 cm at an extension rate of 0.2 mm s^{-1}. The thermal decomposition behavior of the samples was analyzed using thermogravimetry analysis (TG, STA8000, USA) under a nitrogen atmosphere, heating from 50 to 800 °C at a rate of 10 °C min^{-1}. X-ray photoelectron spectroscopy (XPS) was performed on a K-Alpha electron spectrometer (PHI5000 Versaprobe III, Japan) to analyze the chemical bonding state of substances in the composite membrane. Contact angles were measured using the sessile drop method with a 5 mL electrolyte on a contact angle meter (Theta Flex, Gothenburg, Sweden). Zeta potential measurements were carried out on a NanoBrook 90 plus PALS particle size analyzer (NanoBrook 90 Plus Zeta, USA). The $LiPF_6$ in EC: DEC electrolyte without membrane was used as a blank sample. The zeta potentials was then measured after PVDF-CA/Mg-Al(31), PVDF-CA/Mg-Al(21), and PVDF-CA/Mg-Al_2O_3 were immersed in 3 mL $LiPF_6$ in EC: DEC electrolyte for 12 h. The anion-adsorption effect of these membranes was thus verified.

Electrochemical characterizations

The cathode materials were prepared by mixing $LiFePO_4$, PVDF, and Super P powders in an 8:1:1 weight ratio with NMP solvent. The mass loading of the cathode was about 1.9−2.1 mg cm^{-2}. The electrochemical performance of Li/membrane/$LiFePO_4$ half-cells with various membranes was evaluated using CR2032 coin cells. The electrolyte used in this study was 1 mol L^{-1} $LiPF_6$ (in EC:

DEC = 1:1 v/v). Cells were assembled in an argon-filled glove box with low moisture (＜0.1 ppm) and oxygen (＜0.1 ppm). Charging/discharging cycling performance and C-rate capability were tested using a Neware Battery Testing System (BTS-4000, Shenzhen, China) over a voltage range of 2.5–4.2 V at 25 °C, respectively.

The electrochemical stability and Li^+ stripping/plating kinetics were evaluated by cyclic voltammetry (CV) tests and linear sweep voltammetry (LSV) in a two-electrode system. The CV test was performed on SS/membrane/Li cells between 0.2 and 5V with a sweep rate of 1 mV S^{-1} at 25 °C. The LSV test was performed on SS/membrane/Li cells between 3 and 5 V with a sweep rate of 0.1 mV S^{-1} at 25 °C. The electrochemical impedance spectroscopy (EIS) test is performed on Li/membrane/LiFePO4 cells before C−rate of cell cycle.

Calculations

Upon weighing the mass of different membranes before and after immersing them in the electrolyte for 2 h at room temperature, the electrolyte uptake ratio was then calculated using Equation (S1):

$$\eta = \frac{M_2 - M_1}{M_1} \times 100\% \tag{S1}$$

Where M1 and M2 are the weights of the membrane before and after soaking, respectively. Membrane porosity was determined using the n-butanol soaking method, and calculated by following Equation (S2):

$$P = \frac{M_2 - M_1}{\rho \times \mathrm{A} \times D} \times 100\% \tag{S2}$$

Where ρ is the density of the n-butanol solvent, M1 and M_2 are the weights of the membrane before and after soaking for 2 h, and A and D are the area and thickness of the membrane, respectively.

The (EIS) method was used to measure the bulk resistance (R_b) of the SS/membrane/SS cells. The measurements were taken at a voltage amplitude of 5 mV and in a frequency range of 0.1–500 kHz at 25 °C. Using Equation (S3), we calculated the ionic conductivity (σ).

$$\sigma = \frac{D}{R_b \times S} \tag{S3}$$

Where D is the thickness of the membrane, S is the surface area, and R_b is the bulk resistance, respectively.

The t_{Li^+} was evaluated by chronoamperometry and EIS. Specifically, the resistance of the Li/membrane/Li cells before and after polarization was tested by AC impedance. Polarization was completed for 3600 s under a voltage of 10 mV, and it was calculated using the following Equation (S4):

$$t_{Li^+} = \frac{I_S(\Delta \text{V-}I_0R_0)}{I_0(\Delta \text{V-}I_SR_S)} \tag{S4}$$

Where ΔV is 10 mv, I_0, I_S, R_0, and Rs represent the initial current, the steady-state current, the initial resistance, and the steady-state resistance, respectively.

Supplementary Discussions

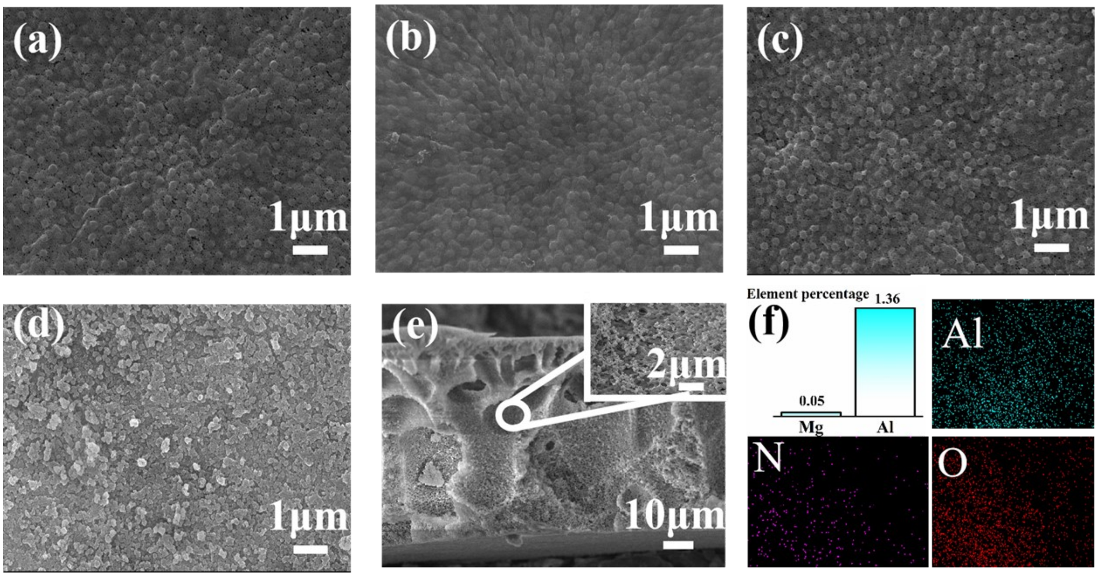

Figure S1. (a-d) SEM images of the backside of PVDF-CA, PVDF-CA/MgO, PVDF-CA/Al_2O_3, and PVDF-CA/Mg-Al_2O_3; (e) SEM images of PVDF-CA/Mg-Al_2O_3 cross-section; (f) ICP and EDS mapping of PVDF-CA/Mg-Al_2O_3 cross-section.

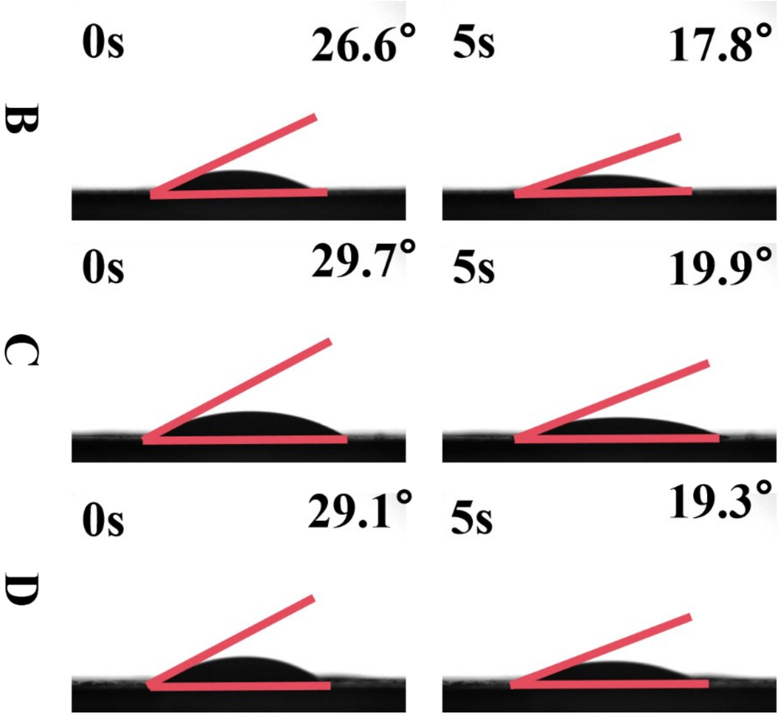

Figure S2. Contact angles of B (PVDF-CA), C (PVDF-CA/MgO), and D (PVDF-CA/Al_2O_3) showing the initial status (left) and latter status after 5s (right).

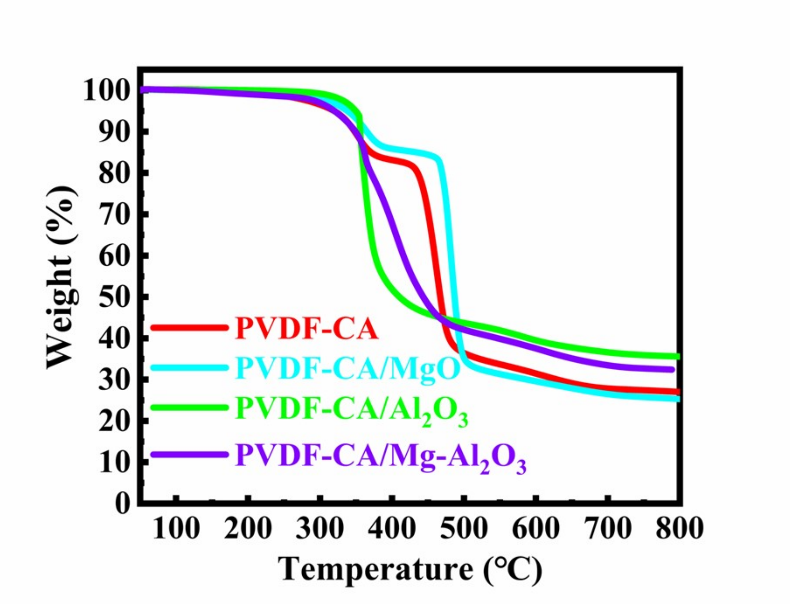

Figure S3. TGA curves of PVDF-CA, PVDF-CA/MgO, PVDF-CA/Al_2O_3, and PVDF-CA/Mg-Al_2O_3.

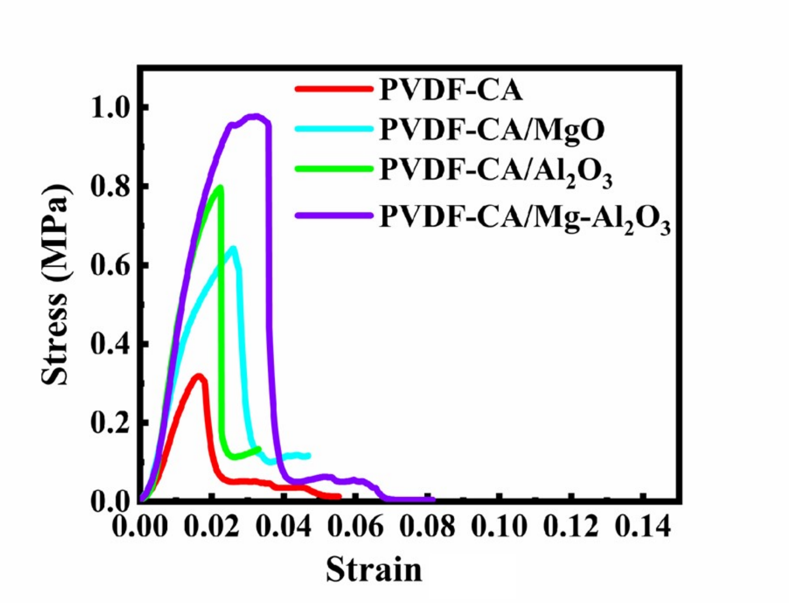

Figure S4. Stress-strain curves of PVDF-CA, PVDF-CA/MgO, PVDF-CA/Al_2O_3, and PVDF-CA/Mg-Al_2O_3.

Various composite membranes were tested by TGA **(Figure S3)**, showing their excellent thermal stability up to 300 °C. Meanwhile, the tensile properties of the composite membranes were tested **(Figure S4)**. The tensile strength and modulus of PVDF-CA/Mg-Al_2O_3 were both higher than other composite membranes.

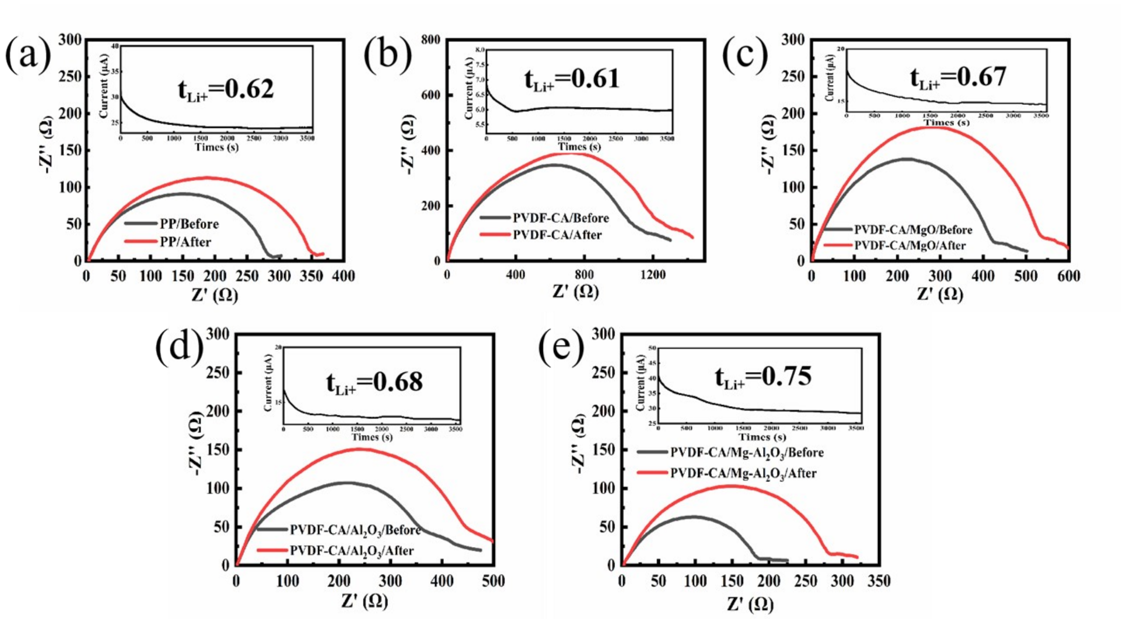

Figure S5. t_{Li}^+ (a) Li/PP/Li cells; (b) Li/PVDF-CA/Li cells; (c) Li/PVDF-CA/MgO/Li cells; (d) Li/PVDF-CA/Al_2O_3/Li cells; (e) Li/PVDF-CA/Mg-Al_2O_3/Li cells.

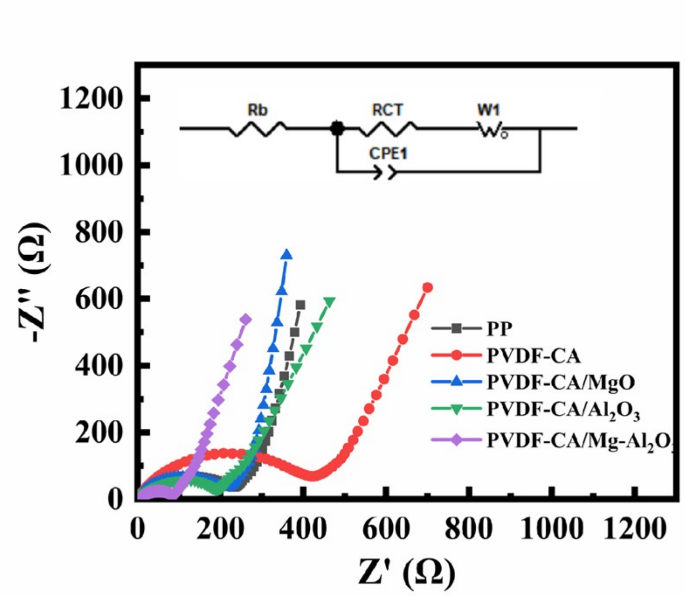

Figure S6. Nyquist plots of Li/membrane/$LiFePO_4$ cells (inset: equivalent circuit for fitting impedance spectra).

AC impedance spectroscopy was utilized to evaluate the interfacial impedance of Li/membrane/$LiFePO_4$ cells assembled with various membranes. As shown in **Figure S6**, the Nyquist plot of the cell with PVDF-CA/Mg-Al_2O_3 exhibit much lower R_{ct} than other cells, indicating efficient Li^+ transport at interfaces.

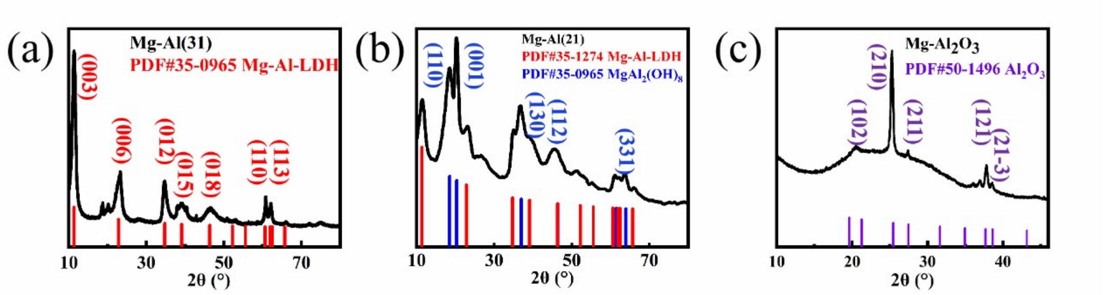

Figure S7. XRD profiles of (a) PVDF-CA/Mg-Al(31); (b) PVDF-CA/Mg-Al(21); (c) PVDF-CA/Mg-Al_2O_3.

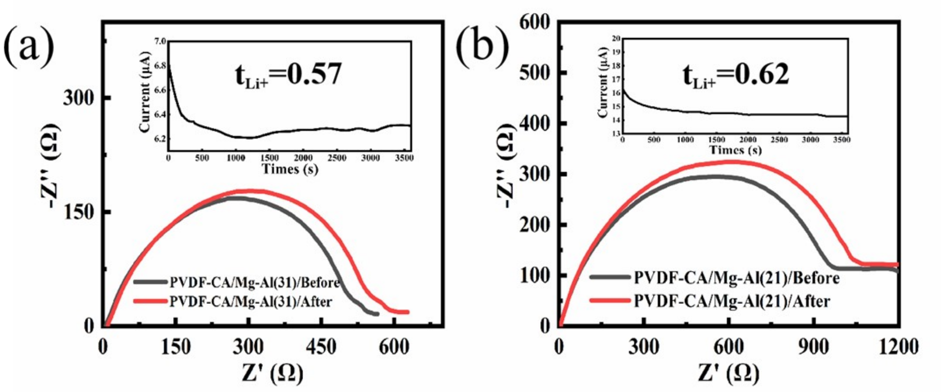

Figure S8. t_{Li}^+ of (a) Li/(PVDF-CA/Mg-Al(31))/Li cells; (b) Li/(PVDF-CA/Mg-Al(21))/Li cells.

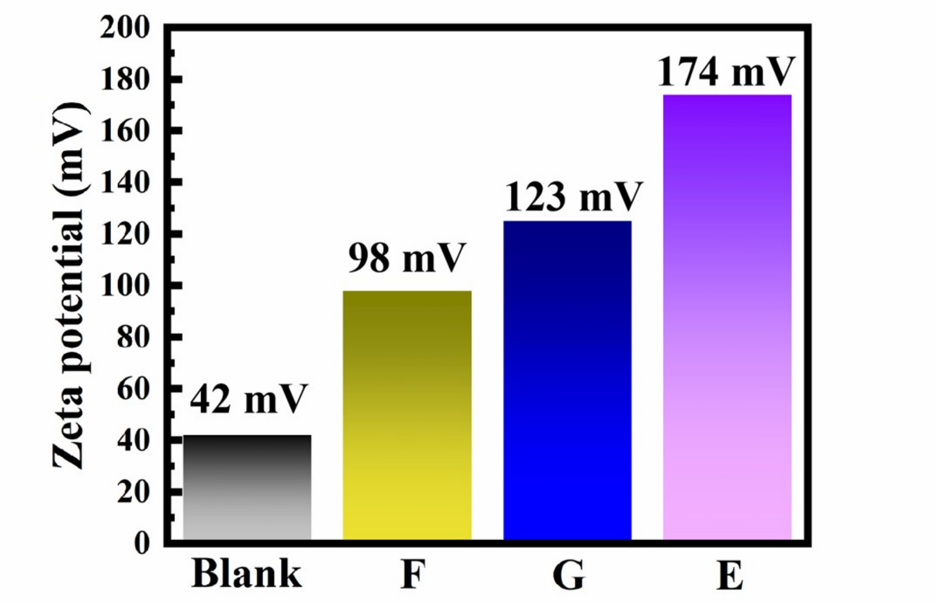

Figure S9. Zeta potentials of the electrolyte (blank) after composite membrane immersion for F (PVDF-CA/Mg-Al(31)), G (PVDF-CA/Mg-Al(21)), and E (PVDF-CA/Mg-Al_2O_3) from left to right.

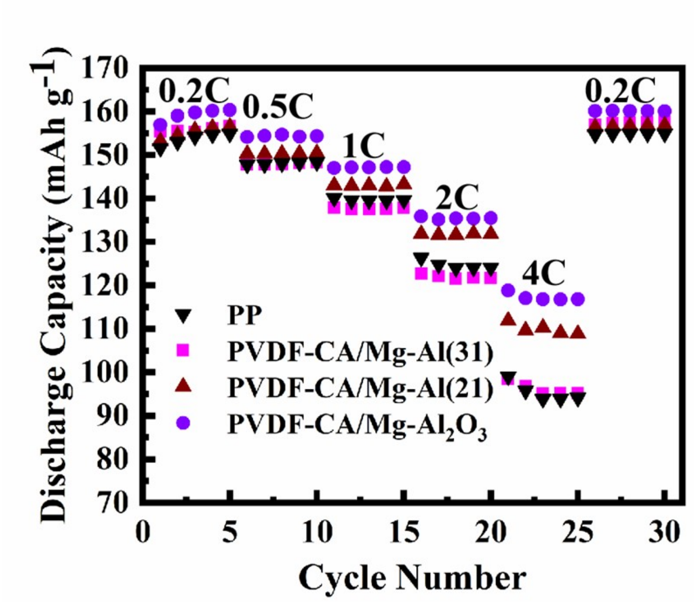

Figure S10. Specific capacity of Li/PP/$LiFePO_4$, Li/(PVDF-CA/Mg-Al(31))/$LiFePO_4$, Li/(PVDF-CA/Mg-Al(21))/$LiFePO_4$, and Li/(PVDF-CA/Mg-Al_2O_3)/$LiFePO_4$ cells at various C-rates.

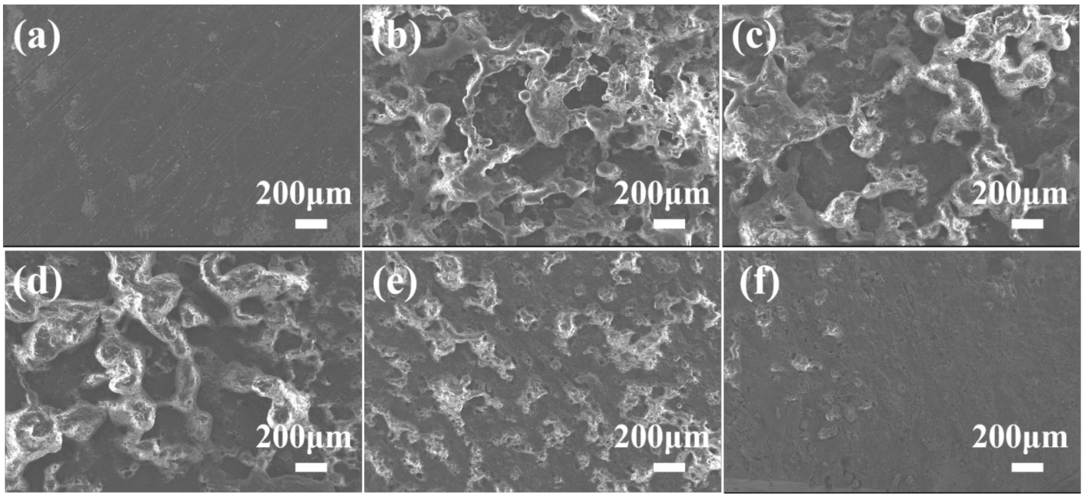

Figure S11. SEM images of Li metal surfaces from Li/membrane/$LiFePO_4$ cells at 1 C-rates (a) before cycling, and after 100 cycles with (b) PP, (c) PVDF-CA, (d) PVDF-CA/MgO, (e) PVDF-CA/Al_2O_3, and (f) PVDF-CA/Mg-Al_2O_3.

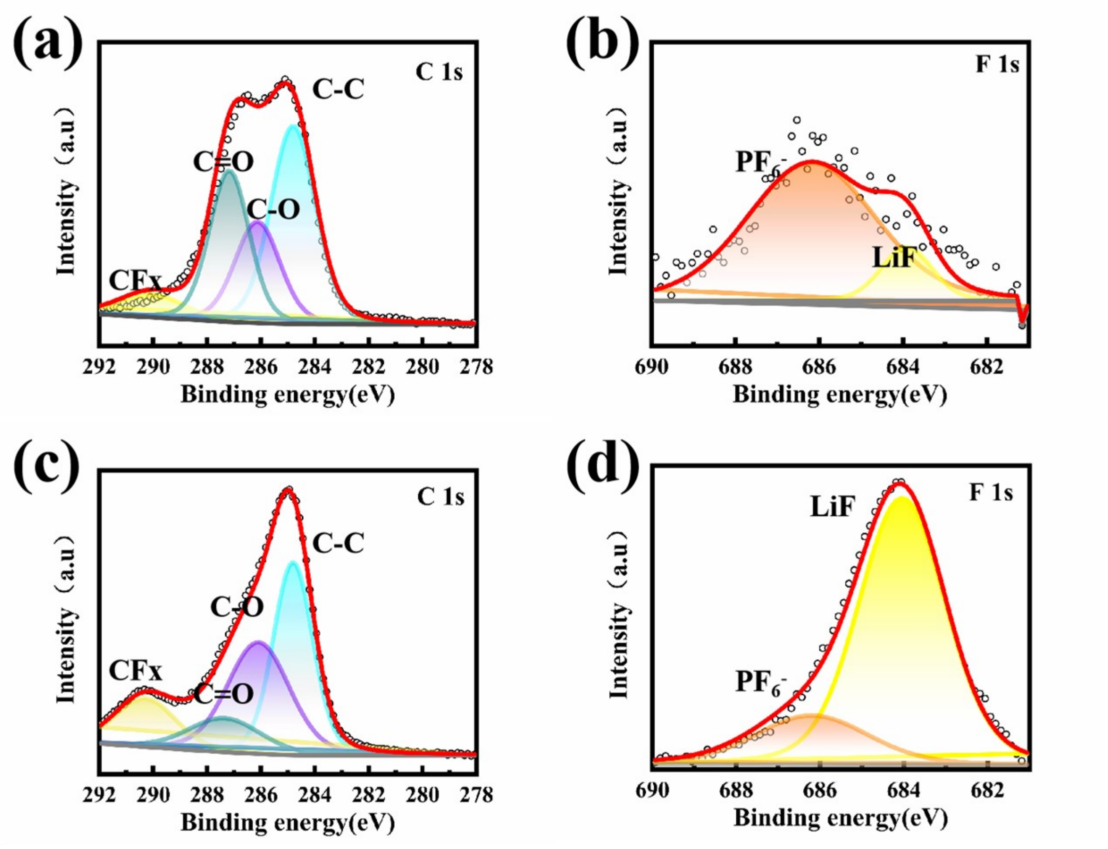

Figure S12. XPS curves of Li metal surfaces from Li/membrane/$LiFePO_4$ cells at 1 C-rates after 100 cycles with (a,b) PP, and (c,d) PVDF-CA/Mg-Al_2O_3.

Furthermore, through the observation of SEM images **(Figure S11)** of Li metal surfaces in the Li/membrane/$LiFePO_4$ cells after 100 cycles at 1C, it is found that the surface of Li metal in the cell employing PVDF-CA/Mg-Al_2O_3 appeared much smoother compared to other cells. This can be attributed to higher ionic conductivity and higher t_{Li^+} of PVDF-CA/Mg-Al_2O_3, significantly mitigating concentration polarization hence slowing down the growth rate of lithium dendrites. XPS analysis was performed on Li metal surfaces after 100 cycles at 1C **(Figure S12)**. In the C 1s spectra, several peaks were observed, including C-C (284.8 eV), C-O (286.1 eV), and C=O (287.3 eV).[2] These peaks are primarily attributed to the organic decomposition products of ethylene carbonate (EC) and diethyl carbonate (DEC). Compared to the cell with PP, organic components in the solid electrolyte interphase (SEI) on Li surface are less for the cell with PVDF-CA/Mg-Al_2O_3. Notably, in the F 1s spectra, the incorporation of in-situ grown nano-Al_2O_3 led to a significant increase in the intensity of the LiF peak (684.1 eV),[3] which is beneficial for the electrochemical stability of the SEI.

Table S1. Bulk resistance (R_b) and ionic conductivity (σ) of symmetrical SS/membrane/SS cells with different membranes.

Name of sample	Thickness of membranes (μm)	R_b (Ω)	σ (mS cm^{-1})
PP	25.0	2.20	0.6
PVDF-CA	77.8	1.63	2.6
PVDF-CA/MgO	85.1	1.59	2.8

PVDF-CA/Al_2O_3	83.0	1.50	2.9
PVDF-CA/Mg-Al_2O_3	84.3	1.38	3.2

Table S2. Specific discharging capacities at different C-rates for Li/membrane/$LiFePO_4$ cells.

Cell	Li/PP/$LiFePO_4$	Li/(PVDF-CA/Mg-Al_2O_3)/$LiFePO_4$
C-rate	Discharging Capacities (mAh g^{-1})	
0.2	157.4	160.2
0.5	151.3	154.3
1.0	141.7	147.2
2.0	126.5	135.4
4.0	94.7	117.1

References (SI)

1. Z. Zheng, L. Lin, S. Mo, D. Ou, J. Tao, R. Qin, X. Fang and N. Zheng, *Small*, 2018, **14**.
2. L. Y. Yang, J. H. Cao, W. H. Liang, Y. K. Wang and D. Y. Wu, *ACS Appl Mater Interfaces*, 2022, **14**, 13722-13732.
3. K. Ma, X. Song, J. Wang, J. Chen, Z. Zheng and J. Zhang, *New Journal of Chemistry*, 2024, **48**, 11282-11292.